sensors

MDPI

Article

Wideband Epidermal Antenna for Medical Radiometry

Germán León [1,*], Luis F. Herrán [1], Ignacio Mateos [2], Enrique Villa [3] and Juan B. Ruiz-Alzola [3,4]

1 Department of Electrical Engineering, Group of Signal Theory and Communications, Universidad de Oviedo, 33202 Gijón, Spain; herranluis@uniovi.es
2 Applied Magnetism and Optics Group, Universidad de Cádiz, 11519 Cádiz, Spain; ignacio.mateos@uca.es
3 IACTec Medical Technology Group, Instituto de Astrofísica de Canarias (IAC), 38205 San Cristóbal de La Laguna, Spain; enrique.villa.benito@iac.es (E.V.); juan.ruiz@ulpgc.es (J.B.R.-A.)
4 Instituto Universitario de Investigación Biomédica y Sanitaria (IUIBS), Universidad de Las Palmas de Gran Canaria (ULPGC), 35001 Las Palmas de Gran Canaria, Spain
* Correspondence: gleon@uniovi.es; Tel.: +34-985-182347

Received: 17 February 2020; Accepted: 30 March 2020; Published: 2 April 2020

Abstract: Microwave thermometry is a noninvasive and passive technique for measuring internal body temperature. Wearable compact antennas, matched to the specific body area, are required for this method. We present a new epidermal wideband antenna for medical radiometry. The double asymmetric H-shaped slot antenna was designed to be matched to different parts of the body without fat layers. The slots are fed by a short-circuited microstrip line in order to decrease size and back radiation, thus reducing potential interferences. In this way, contribution to radiometric temperature due to back radiation is lower than 4%, versus the 20% of the volume under investigation, over the whole operating frequency band. The designed prototype was manufactured on a flexible substrate. The antenna is a very small size, to make it comfortable and suitable for being used by patients with different body mass indexes. The double H-shaped antenna shows good wideband matching results from around 1.5 GHz up to 5 GHz, in different body locations such as the neck, foot instep and foot sole.

Keywords: epidermal antenna; flexible wideband antenna; microwave medical applications

1. Introduction

Medical Microwave Radiometry (MMR) is a low-cost, non-ionizing, non-invasive procedure for medical diagnosis. This passive method is based on the measurement of the internal thermal electromagnetic (EM) radiation of a body region, and its detection using a radiometer system (Figure 1). Hence, the analysis of any anomalous temperature variation measured using these systems could help in the assessment of a medical complication or pathology. Indeed, MMR has already been applied to cancer detection [1], cancer treatment [2], hyperthermia temperature control [3], human core temperature tracking [4], atherosclerosis in the human carotid [5] and the diagnosis of arterial disease in diabetic patients [6]. In all these applications, the MMR system has to be able to detect temperature variations of less than 1 K, and thus, very small changes in the received power. Therefore, an antenna able to measure the EM radiation in an efficient way is required. Hence, it demands a good coupling between the MMR probe and the area under test. In addition, a good matching is also compulsory, which depends on the specific body region and on the patient's complexion, since an adipose layer close to the skin could significantly modify the permittivity of the intended tissue. This is mainly due to the substantially lower value of the relative permittivity of fat tissue compared to skin or muscle.

A great variety of antennas have been developed for medical diagnosis, depending on the body region under test and the working band. Folded antennas are used to reduce size in off-body wideband

systems [7–9]. However, the distance between the antenna and the body is critical for good matching, and they show a poor front-to-back ratio. To overcome these problems and improve the coupling, on-body matched antennas are chosen not only for medical diagnosis [10–13] but also for Wireless Personal Area Network (WPAN) communications [14,15]. In order to increase the efficiency of the measurement system, most of these designs have a reflector to reduce the backward radiation [10,14], but this also increases the complexity. Moreover, wideband epidermal antennas can help MMR, since they can be used to measure below skin surface in multiband applications [3]. Besides, they can help to increase the matching between the device and the subject under test to a larger number of patients [5,6]. However, these antennas are not suitable for wearable devices.

In this work, an epidermal antenna, based on an asymmetric double-H antenna, is proposed for MMR applications, with the goal of evaluating diabetic foot [6] or carotid artery diseases associated with subcutaneous temperature anomalies [5] specifically. The radiating slots are matched through a short-circuited stub to body regions without adipose layers, and the design does not require reflector planes or intermediate matching media to reduce back radiation. Low-profile and easy to manufacture designs have been achieved, so this antenna is a potential candidate as a wearable antenna. The design and radiation characteristics are described in Section 2. A measurement campaign was carried out (Section 3) to show the matching of the antenna in several scenarios between 1.5 and 5 GHz, as well as the low back radiation level. Finally, the main conclusions are summarized in Section 4.

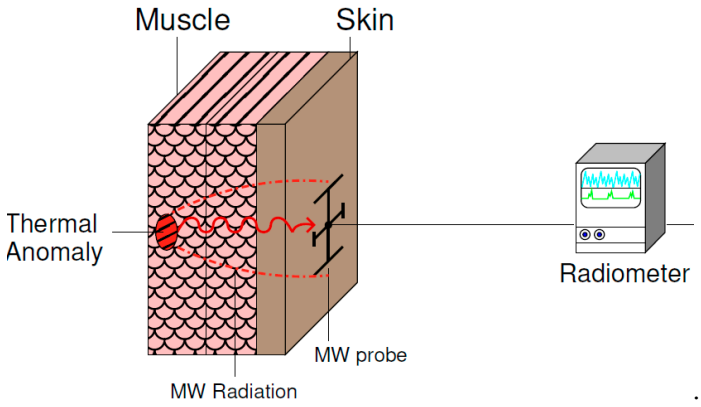

Figure 1. Scheme of the proposed MMR measurement set-up.

2. Wideband Antenna Design

2.1. Short-Circuited Stub Matching

A rectangular slot, placed on the body, can resonate if its length is approximately

$$W_s = \frac{\lambda_{body}}{2} = \frac{c_0}{2f\sqrt{\epsilon_{body}}} \quad (1)$$

where λ_{body} and ϵ_{body} are the effective wavelength and relative permittivity of the body, respectively, and f the operating frequency. In that case, the slot mainly radiates towards the body due to the high contrast between the permittivities of the air and the body. In order to decrease the size of the radiating antenna, an H-shaped slot can be used [16]. Subsequently, a Jerusalem-cross slot can be formed by the combination of two H-shaped slots. A schematic diagram of the proposed antenna is illustrated in Figure 2. The slots are fed by a microstrip line ending in a short circuit to reduce the back radiation, instead of a typical open circuit that produces spurious radiation. The feed line, in the front side of the substrate, and the slots in the backside, form an angle of 45 degrees, to excite both possible resonances. The antenna has been manufactured inside a 25-mm diameter circle, which is small enough to be comfortable for patients. Variations on the ground plane size do not generate changes in the antenna behavior.

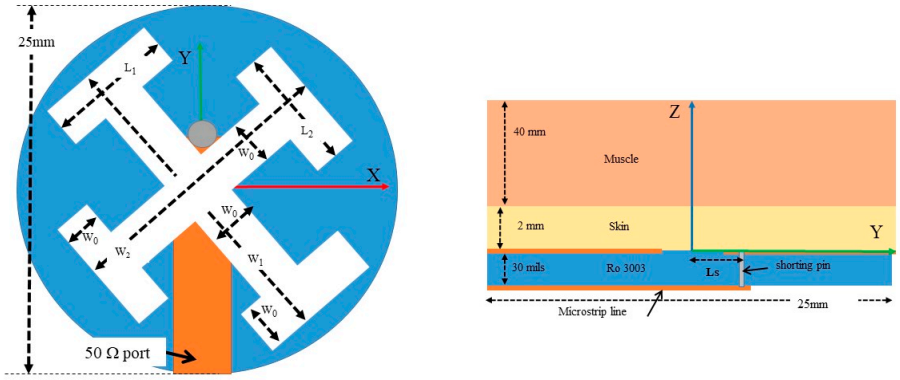

(**a**) (**b**)

Figure 2. Scheme of the asymmetric Jerusalem-cross slot antenna. (**a**) Top view, (**b**) side view.

The antenna must be matched to a human neck [5] or foot [6], which are body areas without an adipose layer. Therefore, a two-layer structure was chosen to model these body volumes. The antenna was in contact with a 2-mm thick skin layer. The second layer (muscle) was modeled as a large enough volume to be considered semi-infinite (Figure 2b). Then, a 40-mm thickness was considered. Since the dielectric properties of the tissues change with frequency, according Table 2 [17], several simulations were carried out using these parameters. The antenna was designed on a Rogers3003^{TM} flexible substrate, with relative permittivity $\epsilon_r = 3.0$, loss tangent $tan\delta = 0.0013$ at 10 GHz, and a thickness of $h = 30$ mils. The design parameters of the antenna were optimized with HFSS [17] and are shown in Table 1. The set of parameters $W_1 + L_1$ and $W_2 + L_2$ control the resonant frequencies of each slot, in agreement with Equation (1), while the parameters W_0 and L_s adjust the matching between the antenna and the body region. In the simulations, a frequency-dependent Debye model was used, with the dielectric properties given in Table 2.

In order to show the better performance of a short-circuited stub versus an open-ended version, the input reflection coefficients of the antenna, using both configurations, are compared in Figure 3. The parameter L_s was fitted to the maximum value for the open stub configuration, that is, L_s = 12 mm. The short-circuited antenna shows a good matching from 1.5 GHz up to more than 5 GHz. This result is much better than the open stub design. To improve the matching for the open-circuited antenna, the surface of the antenna has to be enlarged, reducing its potential use as an epidermal antenna.

Table 1. Design Parameters of the Jerusalem Cross Antenna (in mm).

W_1	W_2	L_1	L_2	L_s	W_0
11.0	6.0	8	4	1.4	1.2

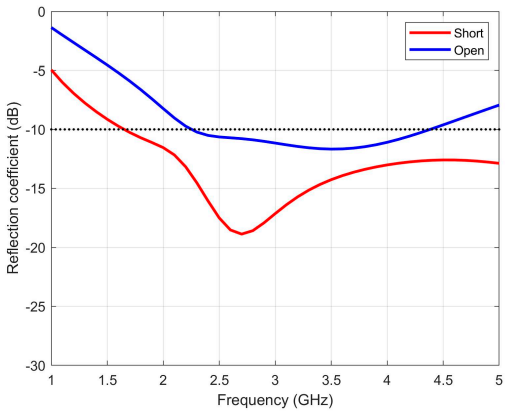

Figure 3. Simulated reflection coefficients of the asymmetric Jerusalem cross slot antenna.

Table 2. Dielectric properties of the tissues [18].

Tissue	Frequency (GHz)	ε_r	σ (S/m)
Wet Skin	2	43.6	1.34
Wet Skin	4	40.8	2.70
Muscle	2	53.3	1.45
Muscle	4	50.8	3.02

2.2. Losses in the Volume

In [4], a microwave radiometer model for body temperature is sketched. In this approach, the temperature of each layer is weighted by a function W_i, which depends on the frequency and conductivity of each tissue layer. Then, the whole body temperature defined by this model is expressed as

$$T = \sum_{i=1}^{N} W_i T_i \tag{2}$$

where T_i is the i-th layer, N is the total number of layers, and T is the radiometric temperature at the probe. The weighting functions can be quantified, by reciprocity, as the relation between the power absorbed by the layer (P_{di}), integrating the volume power loss density of each layer (D_i) and the total power (P) provided by the feed. The weighting function of a layer placed between $0 < Z_1 < Z_2$ can be calculated as

$$W_i = \frac{P_{di}}{P} = \frac{\int_{Z_1}^{Z_2} \int_{-\infty}^{\infty} \int_{-\infty}^{\infty} D_i(x,y,z)dxdydz}{P} \tag{3}$$

It has to be highlighted that in this equation, the matching of the antenna is taken into account.

In [4], back radiation contribution is not taken into account. However, it is easy to add another term to Equation (2) to estimate the contribution of the temperature radiation of the lab (T_{lab}), with a weighting function W_{back}, integrating the radiation at a semi-sphere in the open air:

$$W_{back} = \frac{P_{back}}{P} = \frac{\int_0^{2\pi} \int_{\pi/2}^{\pi} \frac{|E(R,\theta,\phi)|^2}{2\eta_0} R^2 sin\theta d\theta d\phi}{P} \tag{4}$$

In Figure 4, volume power losses for different frequencies inside the proposed phantom model tissues (Figure 2b) are shown in plane Y = 0. In all frequencies, the antenna is fed by a power of 1 W. Although the propagation losses inside the tissue increase with frequency, the E-field remains approximately constant. This is because the electrical size of the antenna also increases with the frequency, and thus the antenna directivity. Similar results were found for the plane $X = 0$.

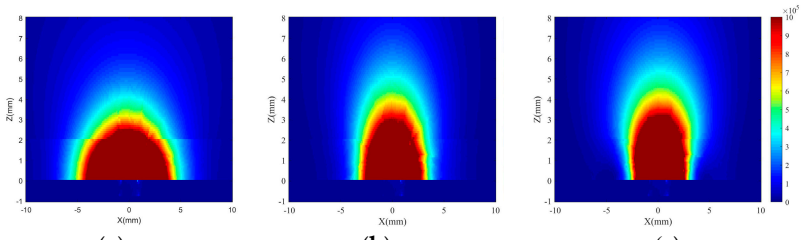

Figure 4. Simulated volume loss density (W/m^3) in the plane Y = 0 of the asymmetric Jerusalem cross antenna, fed by a power of 1 W at (**a**) 2 GHz, (**b**) 3 GHz, and (**c**) 4 GHz.

These figures also show that the losses inside the substrate ($0 < Z < -30$ mils) are negligible. The electromagnetic properties of the tissues (skin and muscle) are very similar, so a slight discontinuity can be seen at $Z = 2$ mm.

The simulated back radiation total electric field for the two principal cuts of the wideband antenna results are shown in Figure 5. The back radiation of the antenna increases at frequencies higher than 4 GHz due to the bigger slot (corresponding to W_1 and L_1 parameters), and begins to radiate to the free space. The back radiation gain has a minimum of 3 GHz and remains below −18 dBi in the whole band. These results ensure very low interferences coming from outside the tissues, between 1.5 GHz and 4 GHz.

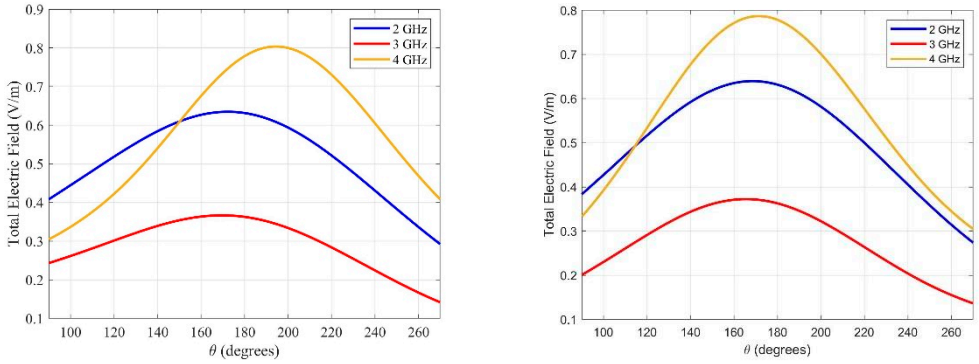

Figure 5. Back radiation electric field of the asymmetric Jerusalem cross antenna for (**a**) $\phi = 0°$ and (**b**) $\phi = 90°$ at different frequencies.

With these values, the weighting functions of each contribution can be calculated, using Equations (3) and (4). We consider our volume under investigation (VUI) to be the muscle slab from depth 3 mm to 7 mm. The whole model [5] consists of a deeper slab (depth > 7 mm), the VUI (depth 3–7 mm) and the skin (depth < 3 mm). We show the simulated weights corresponding to the contribution of each slab, and the back radiation for the temperature formation model (Equation (2)) in Table 3, along with the simulated specific absorption rate (SAR) in the skin, which may be taken as a reference for future applications with radiating antennas. SAR has been calculated for the skin tissue (with density of 1125 Kg/m^3) when the antenna is fed with a power of 15 mW. This power is within SAR values used in the standard presented in [19] at this frequency band.

Table 3. Calculated weighting functions and SAR for the skin, for a power of 15 mW.

Frequency	Back-Rad. W_{back}	W_1 (0–3 mm)	W_2 (3–7 mm) (VUI)	W_3 (Z > 7 mm)	Skin SAR (W/kg)
2 GHz	0.028	0.571	0.165	0.173	15.4
3 GHz	0.009	0.623	0.195	0.163	16.5
4 GHz	0.036	0.668	0.175	0.071	18.0

As expected, the higher losses are found in the superficial layer. This value increases with frequency. The contribution of the VUI is enough to detect temperature changes of about 1 K. The back radiation contribution remains low enough, so changes in laboratory temperature do not influence the radiometric measurement. From 4 GHz, the back radiation losses increase, and the contribution of the VUI decreases. For this reason, it is recommending to use the probe up to 4 GHz for medical radiometry, although the antenna is matched.

3. Experimental Validation

Two antennas have been manufactured to validate the characteristics of the described design (Figure 6). In order to demonstrate the matching of the antenna, measurements on four volunteers with different body mass indices (BMI, Table 4) have been performed to show the behavior of the antenna on the body area under test.

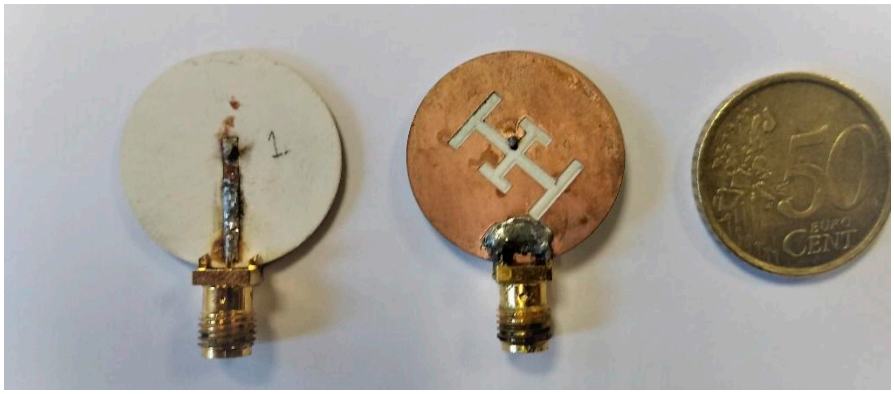

Figure 6. Manufactured prototypes.

Table 4. Body Mass Index of the Volunteers.

Volunteer	Gender	BMI	Foot Size (cm)
S1	Female	17.4	25.5
S2	Female	21.8	22.5
S3	Male	30.2	29
S4	Male	18.3	27.5

3.1. Matching Measurement Campaign

The measured reflection coefficients of the antenna are presented in Figures 7–9, for each one of the mentioned body areas.

The behavior of the antenna on the carotid (Figure 7) is very similar for the four volunteers. In all cases, the antenna is well matched in the whole required band (between 1.5 GHz and 5.0 GHz), with values below −10 dB between 1.6 GHz to 4.5 GHz in all cases. Moreover, the measured results are very similar to the simulated ones.

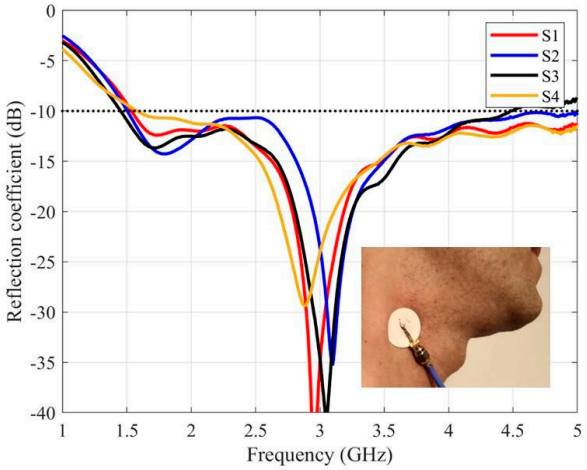

Figure 7. The measured reflection coefficients of the purposed antenna placed on the carotid.

In Figure 8, results for the instep are shown. In this case, the antenna is also matched in three cases, from 1.8 GHz, while for the S2 volunteer, the antenna is slightly mismatched around 2.2 GHz.

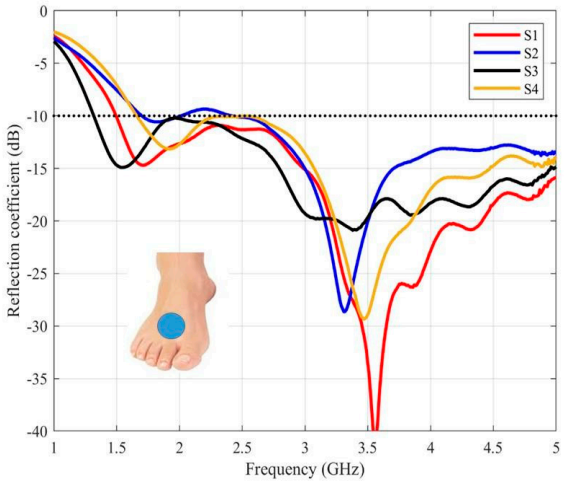

Figure 8. The measured reflection coefficients of the purposed antenna placed on the instep.

The more significant difference has appeared in the sole area (Figure 9) for one of the volunteers (S2). In this particular case, the subject under test presents the smallest foot (Table 4) which hinders the matching of the antenna.

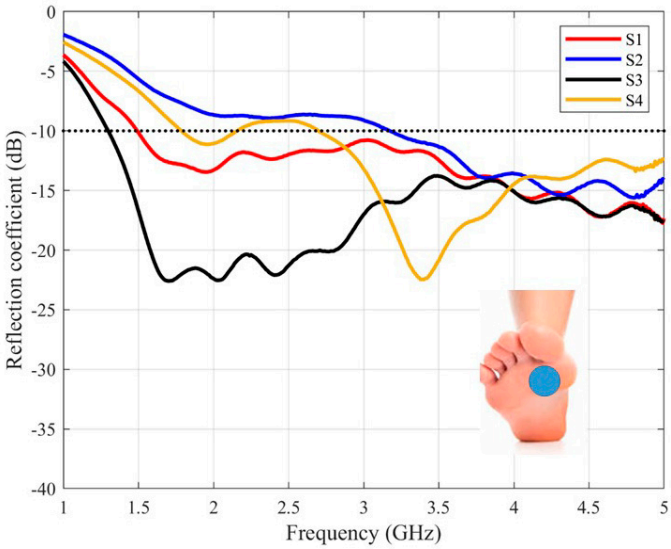

Figure 9. The measured reflection coefficients of the purposed antenna placed on the sole.

3.2. Back radiation Measurement Campaign

In order to show the back radiation level of the designed antenna, an *ex profeso* measurement set-up has been developed. The antenna under test was placed on a mimic gel made with MSL900V2 solution [20] with ε_r = 46.50 and σ = 2.28 S/m at 2 GHz, agar-agar as a gelling agent, and red colorant. The antenna is matched between 1.5 and 5 GHz (Figure 10a). The measured reflection coefficient is very similar to the simulated one, using the proposed model. The antenna on the gel was positioned in an anechoic planar range facility (Figure 10b), and a vector network analyzer was used to measure the transmission coefficient between the antenna under test and the probe antenna.

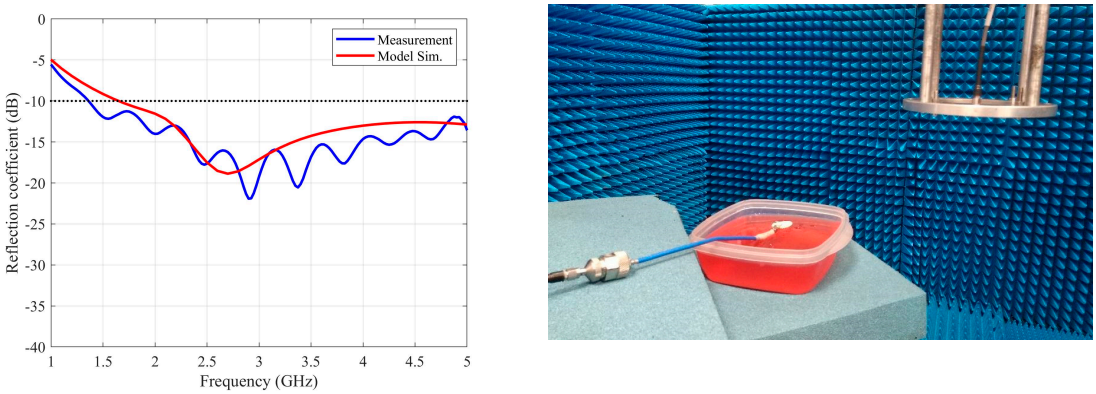

Figure 10. (**a**) Measurement and simulation of the reflection coefficient of the antenna under test (**b**) Back radiation measurement set-up.

At working frequencies, typical near field probes based on open waveguides are bulky and heavy. Because of this, two sets of patch antennas matched at 2, 3 and 4 GHz were manufactured. At these frequencies, the antennas exhibit a gain of 4.1, 5.0 and 5.9 dBi respectively. One set was used as the probe antenna, while the other was used as the reference.

The transmission coefficient along the *X-axis* was simulated and measured for the antenna under test and the reference antennas at a distance of 155 mm. The results were normalized to the transmission coefficient of an isotropic radiator and they are plotted in Figure 11. For all the considered frequencies, the maximum radiation is below −20 dBi, being, in the worst case, 4 GHz, as was predicted in the previous section. Similar results were found in measurement along the *Y-axis*. These results confirm the low level of back radiation of the purposed antenna.

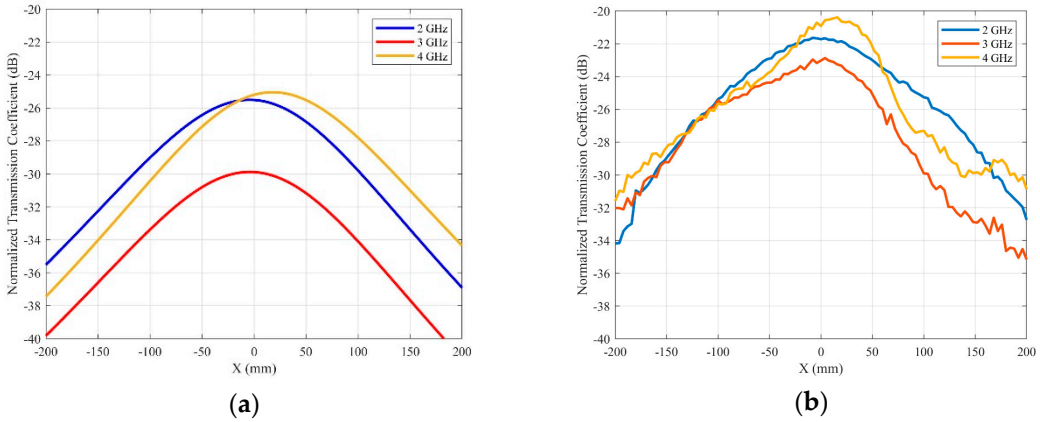

Figure 11. Normalized transmission coefficient for the back radiation of the Jerusalem cross slot antenna. (**a**) Simulations. (**b**) Measurements.

4. Conclusions

In this work, an epidermal wideband antenna for medical radiometry is presented. Body areas without adipose layers, such as the neck or foot, are intended as matching body tissues. A new, compact, low-profile and low-cost antenna, based on two radiating slots over a flexible substrate layer, was designed and validated. The antenna can reduce the backward radiation by using a short-circuited stub. The manufactured prototype was proved with four different volunteers, matched to body areas such as the carotid, the instep, and the sole of the foot. In all cases, the antenna was matched, showing a wideband performance between 1.8 and 5 GHz, that is around a 100% relative bandwidth. In addition, the antenna has very low back radiation up to 4 GHz, which reduces interferences and minimizes its

contribution to the radiometric temperature. A measurement campaign in an anechoic facility was carried out, and it was shown that the normalized transmission coefficients are below −20 dBi in all cases. The designed antenna is easy to manufacture and comfortable for patients. It has a simple and flexible design to be used on other areas of the body, and it could be easily integrated into wearable microwave sensors.

Author Contributions: Conceptualization, G.L., I.M. and J.B.R.-A.; simulation and validation, G.L. and L.F.H.; writing—original draft preparation, G.L. and L.F.H.; writing—review and editing, visualization and supervision, I.M., E.V. and J.B.R.-A. All authors have read and agreed to the published version of the manuscript.

Funding: This work was supported in part by the Ministerio de Ciencia e Innovación, under project TEC2017-86619-R (ARTEINE) and Consejería de Empleo, Industria y Turismo under project GRUPIN-IDI-2018-000191.

Conflicts of Interest: The authors declare no conflict of interest. The funders had no role in the design of the study; in the collection, analyses, or interpretation of data; in the writing of the manuscript, or in the decision to publish the results.

References

1. Carr, K.L. Microwave radiometry: Its importance to the detection of cancer. *IEEE Trans. Microw. Theory Technol.* **1989**, *37*, 1862–1869. [CrossRef]
2. Shaeffer, J.; El-Mahdi, A.M.; Hamwey, A.E.; Carr, K.L. Detection of extravasation of antineoplastic drugs by microwave radiometry. *Cancer Lett.* **1986**, *31*, 285–291. [CrossRef]
3. Jacobsen, S.; Stauffer, P.R. Multifrequency radiometric determination of temperature profiles in a lossy homogeneous phantom using a dual-mode antenna with integral water bolus. *IEEE Trans. Microw. Theory Technol.* **2002**, *50*, 1737–1746. [CrossRef]
4. Momenroodaki, P.; Haines, W.; Fromandi, M.; Popovic, Z. Noninvasive internal body temperature tracking with near-field microwave radiometry. *IEEE Trans. Microw. Theory Technol.* **2018**, *66*, 2535–2545. [CrossRef]
5. Toutouzas, K.; Grassos, C.; Drakopoulou, M.; Synetos, A.; Tsiamis, E.; Aggeli, C.; Stathogiannis, K.; Klettas, D.; Kavantzas, N.; Agrogiannis, G.; et al. First in vivo applications of microwave radiometry in human carotids. A new noninvasive method for detection of local inflammatory activation. *J. Am. Coll. Cardiol.* **2012**, *59*, 1645–1653. [CrossRef] [PubMed]
6. Spiliopoulos, S.; Theodosiadou, V.; Barampoutis, N.; Katsanos, K.; Davlouros, P.; Reppas, L.; Kitrou, P.; Palialexis, K.; Konstantos, C.; Siores, E.; et al. Multi-center feasibility study of microwave radiometry thermometry for non-invasive differential diagnosis of arterial disease in diabetic patients with suspected critical limb ischemia. *J. Diabetes Complicat.* **2017**, *31*, 1109–1114. [CrossRef] [PubMed]
7. Mobashasher, A.T.; Bialkowski, K.S.; Abbosh, A.M. Design of compact cross-fed three-dimensional slot-loaded antenna and its application in wideband head imaging system. *IEEE Antennas Wirel. Propag. Lett.* **2016**, *15*, 1856–1860. [CrossRef]
8. Rezaeieh, S.A.; Abbosh, A.M. Wideband and unidirectional folded antenna for heart failure detection system. *IEEE Antennas Wirel. Propag. Lett.* **2014**, *13*, 844–847. [CrossRef]
9. Mobashsher, A.; Abbosh, T.A. Slot-loaded folded dipole antenna with wideband and unidirectional performance for L-Band applications. *IEEE Antennas Wirel. Propag. Lett.* **2014**, *13*, 798–801. [CrossRef]
10. Zheng, C.; Jiang, X.; Kang, B.; Li, X.; Geng, Z. Design of an on-body matched wide-slot UWB Antenna for brain activities detection. In Proceedings of the Sixth Asia-Pacific Conference on Antennas and Propagation (APCAP), Xi'an, China, 16–19 October 2017. [CrossRef]
11. Tømmer, M.; Kjelgard, K.G.; Lande, T.S. Body-Coupled wideband monopole antenna. In Proceedings of the Loughborough Antennas & Propagation Conference (LAPC), Loughborough, UK, 14–15 November 2016. [CrossRef]
12. Li, X.; Jalilvand, M.; Sit, Y.; Zwick, T. Compact double-layer on-body matched bowtie antenna for medical diagnosis. *IEEE Trans. Antenna Propag.* **2014**, *62*, 1808–1816. [CrossRef]
13. Klemetsen, Ø.; Jacobsen, S. Improved radiometric performance attained by an elliptical microwave antenna with suction. *IEEE Trans. Biomed. Eng.* **2012**, *59*, 263–271. [CrossRef] [PubMed]
14. Zebiri, C.; Sayad, D.; Elfergani, I.; Iqbal, A.; Mshwat, W.F.; Kosha, J.; Rodriguez, J.; Abd-Alhameed, R. A Compact Semi-Circular and Arc-Shaped Slot Antenna for Heterogeneous RF Front-Ends. *Electronics* **2019**, *8*, 1123. [CrossRef]

15. Di Serio, A.; Buckley, J.; Barton, J.; Newberry, R.; Rodencal, M.; Dunlop, G.; O'Flynn, B. Potential of Sub-GHz Wireless for Future IoT Wearables and Design of Compact 915 MHz Antenna. *Sensors* **2018**, *18*, 22. [CrossRef] [PubMed]
16. León, G.; Boix, R.R.; Medina, F. A comparison among different reduced-size resonant microstrip patches. *Microw. Opt. Technol. Lett.* **2001**, *29*, 143–146. [CrossRef]
17. Ansys HFSS Software, Version 19.2. Available online: http://www.ansys.com/ (accessed on 10 February 2020).
18. Dielectric Properties of Body Tissues. Available online: http://niremf.ifac.cnr.it/tissprop/ (accessed on 10 February 2020).
19. International Commission on Non-Ionizing Radiation Protection. Guidelines for limiting exposure to time-varying electric, magnetic, and electromagnetic fields (up to 300 GHz). *Health Phys.* **1998**, *74*, 494–522.
20. SPEAG. Available online: www.speag.swiss (accessed on 10 February 2020).